Spin texturing in a parabolically confined quantum wire with Rashba and Dresselhaus spin–orbit interactions*

S. Sarıkurt[a)b)†], S. Şakiroğlu[b)], K. Akgüngör[b)], and İ. Sökmen[b)]

[a)] *Dokuz Eylül University, The Graduate School of Natural and Applied Sciences, Physics Department, Tınaztepe Campus, 35390, İzmir, Turkey*
[b)] *Dokuz Eylül University, Faculty of Science, Physics Department, Tınaztepe Campus, 35390 İzmir, Turkey*

(Received 31 May 2013; published 3 December 2013)

In this study, we investigate theoretically the effect of spin–orbit coupling on the energy level spectrum and spin texturing of a quantum wire with a parabolic confining potential subjected to the perpendicular magnetic field. Highly accurate numerical calculations have been carried out using a finite element method. Our results reveal that the interplay between the spin–orbit interaction and the effective magnetic field significantly modifies the band structure, producing additional subband extrema and energy gaps. Competing effects between external field and spin–orbit interactions introduce complex features in spin texturing owing to the couplings in energy subbands. We obtain that spatial modulation of the spin density along the wire width can be considerably modified by the spin–orbit coupling strength, magnetic field and charge carrier concentration.

Keywords: spin–orbit coupling, zeeman splitting, quantum wire, spin texture

PACS: 71.70.Ej, 75.70.Tj, 73.21.Hb, 85.75.–d **DOI:** 10.1088/1674-1056/23/1/017102

1. Introduction

Spintronics is an ever-evolving research field of magnetic electronics which uses the spin of electrons rather than its charge to store the data.[1] The aim of this multidisciplinary field is to understand the interaction between the particle's spin and its solid-state environment and to produce useful devices (e.g., spin-FETs (field effect transistors), MRAM (magnetoresistive random-access memory), etc.) based on spin dynamics.[2,3]

In spin-based semiconductor devices, spin–orbit (SO) interaction is considered an important tool for controlling and manipulating the spin orientation.[4–6] Inversion asymmetry properties of low-dimensional systems give rise to the Rashba[7,8] and Dresselhaus[9] SO couplings. Rashba SO coupling arises due to structure inversion asymmetry along the growth direction in quantum heterostructures where two-dimensional electron gas (2DEG) is realized. Dresselhaus SO coupling arises due to bulk inversion asymmetry of the lattice.[10–12] The Dresselhaus term has two components, one linear in the momentum and the other cubic. The cubic term is usually neglected, since it is generally smaller than the linear one.[13] The strength of the Rashba SO coupling can be tuned by changing the gate voltage,[14] whereas the Dresselhaus SO coupling contribution can be tuned by the sample thickness or electron density.[15,16] The strengths of the SO terms are difficult to measure independently, but a full understanding of their strengths is crucial[17] for investigations of spin dependent phenomena in low-dimensional structures.[14,18,19]

Spin density modulation emerged in quantum confined systems known as the "spin texturing effect", which is important for spintronics due to the fact that it provides information about the spatial distribution of the effective magnetic field in the presence of SO interaction.[20,21] In recent years, investigations of SO coupling effects in low-dimensional systems have attracted a considerable amount of interest. There are many theoretical[20,22,23] and experimental works which survey extensively the effects of SO coupling on the electronic and transport properties of these systems. Moroz and Barnes[24,25] and Mireles and Kirczenow[26] theoretically calculated the influence of Rashba SO interaction on the band structure and transport at low temperatures of quasi-one-dimensional (1D) electron systems. Perroni *et al.*[27] discussed spectral and the transport properties of a quasi-1D quantum wire with hard-wall boundaries in the presence of Rashba SO interaction while Pramanik *et al.*[28] numerically calculated the energy dispersion relations and spatial variation of spin components of InAs quantum wire in the presence of both SO interactions. More recently, Gujarathi *et al.*[21] reported the subband structure and spatial modulation of the spin density in a quantum wire with hard-wall confinement for a wide range of magnetic field, Dresselhaus SO coupling strength and carrier concentration. The electronic structure of Rashba spin–split quantum wire that is parabolically confined under the influence of a perpendicular magnetic field has been studied by Knobbe and Schäpers[6] and Debald and Kramer.[14] Furthermore, Zhang *et al.*[5] obtained the energy band structure of quantum wires described by a parabolic confinement potential and subjected to an external magnetic field taking into account both Rashba

*Project supported by Research Grants DEU-BAP:2009183 and DEU-BAP:2009184 from Scientific Research Fund of Dokuz Eylül University.
†Corresponding author. E-mail: sevil.sarikurt@deu.edu.tr
© 2014 Chinese Physical Society and IOP Publishing Ltd

and Dresselhaus SO interactions. In Ref. [29], researchers reported that the interplay of Rashba, Dresselhaus and the lateral SO interaction as well as the applied magnetic field in a parabolic quantum wire lead to rather complex electrosubbands. An analytical approximation scheme suitable for obtaining the energy spectrum of a quasi-1D (one dimensional) quantum wire with SO coupling has been developed by Erlingsson *et al.*[30] and Gharaati and Khordad.[31] Experimental works have been performed by several researchers. The effect of Rashba SO coupling in InGaAs/InP quantum wire structures has been discussed in Refs. [32]–[34]. On the other hand, in Ref. [15] the effects of both SO coupling terms in 2DEG and quantum wire structures have been investigated.

Although there are several works related to Rashba and Dresselhaus SO interactions in quantum confined systems, to our knowledge, less attention has been paid on the spin texture calculations for parabolically confined quantum wires in an external magnetic field. Detailed investigation of electrosubbands and spin density modulation could be useful for identification of spin polarization in zinc-blende quantum wires. In this study, we calculate the energy spectrum of spin–split subbands and spin orientations of a parabolic quantum wire considering various strengths of Rashba and Dresselhaus SO couplings and the external perpendicular magnetic field for different carrier concentrations.

The organization of the paper is as follows. In Section 2, we briefly outline the physical model and the formulation of the system. The numerical results and discussion are presented in Section 3 and finally, we conclude in Section 4.

2. Model and method

We consider a quasi-1D quantum wire with SO interaction in a perpendicular magnetic field. We assume that the wire material is GaAs so that the effective mass of electrons is 0.067 times the free electron mass ($m^* = 0.067m_0$) and the effective Lande-g factor $g^* = -0.44$. We assume that the wire lies in the xy plane with $\hat{y}$ direction parallel to the wire and has a parabolic confinement in the $\hat{x}$ direction $V_{\rm conf}(x) = (m^*/2)\omega_0^2 x^2$ (Fig. 1). Charge carriers move freely along the y direction, accordingly translational invariance along this direction exists. The magnetic field is oriented along the growth direction, taken to be $\hat{z}$, $\boldsymbol{B} = (0,0,B)$, with corresponding magnetic vector potential in Landau gauge expressed as $\boldsymbol{A} = (0,Bx,0)$.

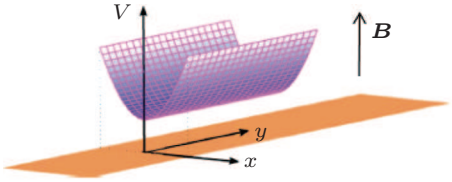


Fig. 1. (color online) Schematic representation of the wire system.[5]

The single particle Hamiltonian in quasi-1D with SO coupling is given by

$$\mathcal{H} = \mathcal{H}_0 + \mathcal{H}_{\rm Z} + \mathcal{H}_{\rm so}. \tag{1}$$

The first term in Eq. (1) contains kinetic energy and confining potential $V_{\rm conf}(x)$ contributions

$$\mathcal{H}_0 = \left\{ \frac{1}{2m^*}\left[p_x^2 + (p_y + eBx)^2\right] + V_{\rm conf}(x) \right\} \sigma_0, \tag{2}$$

where p_x, p_y are components of electron momentum and σ_0 is the 2×2 unit matrix. The second term is the Zeeman Hamiltonian, which is known as

$$\mathcal{H}_{\rm Z} = \frac{1}{2} g^* \mu_{\rm B} \sigma_z B, \tag{3}$$

where g^* is the effective Lande-g factor, $\mu_{\rm B}$ is the Bohr magneton and σ_z is the z component of the Pauli spin matrix. The last term $\mathcal{H}_{\rm so}$ is the total SO Hamiltonian, which involves Rashba and Dresselhaus SO couplings

$$\mathcal{H}_{\rm so} = \mathcal{H}_{\rm R} + \mathcal{H}_{\rm D}.$$

The Rashba SO Hamiltonian is given by

$$\mathcal{H}_{\rm R} = \frac{\alpha}{\hbar}\left[\sigma_x(p_y + eBx) - \sigma_y p_x\right], \tag{4}$$

whereas the Dresselhaus SO Hamiltonian is

$$\mathcal{H}_D = \frac{\beta}{\hbar}\left[\sigma_y\,(p_y + eBx) - \sigma_x\; p_x\right]. \tag{5}$$

Here, α and β represent the Rashba and Dresselhaus SO coupling parameters, respectively, σ_x and σ_y denote the Pauli spin matrix components.

Translational invariance along the $\hat{y}$ direction allows us to decompose the eigenfunction of total Hamiltonian (1) into plane waves in the longitudinal direction and a spinor part depending on the transverse coordinate x, such as

$$\Psi(x,y) = \mathrm{e}^{\mathrm{i}k_y y}\begin{pmatrix} \varphi_\uparrow(k_y,x) \\ \varphi_\downarrow(k_y,x) \end{pmatrix} =: \mathrm{e}^{\mathrm{i}k_y y}\varphi(x), \tag{6}$$

where wave numbers k_y are good quantum numbers of the system. With this wave function ansatz, the Schrödinger equation becomes separable in x and y. Therefore, the explicit form of the $\mathcal{H}_0$ and $\mathcal{H}_{\rm so}$ Hamiltonians can be written as follows:

$$\mathcal{H}_0 = \left[-\frac{\hbar^2}{2m^*}\frac{\mathrm{d}^2}{\mathrm{d}x^2} + \frac{1}{2}m^*\omega^2(x-x_0)^2 + \frac{\omega_0^2}{\omega^2}\frac{\hbar^2 k_y^2}{2m^*}\right]\sigma_0, \tag{7}$$

$$\mathcal{H}_{\rm so} = \alpha\left[\sigma_x\left(k_y + \frac{eB}{\hbar}x\right) + \mathrm{i}\sigma_y\frac{\mathrm{d}}{\mathrm{d}x}\right] + \beta\left[\sigma_y\left(k_y + \frac{eB}{\hbar}x\right) + \mathrm{i}\sigma_x\frac{\mathrm{d}}{\mathrm{d}x}\right], \tag{8}$$

where $\omega = (\omega_0^2 + \omega_{\rm c}^2)^{1/2}$ is the effective oscillator frequency with the cyclotron frequency $\omega_{\rm c} = eB/m^*$, $x_0 =$

$-(\omega_c/\omega)^2(\hbar k_y/eB) = -(\omega_c\omega_0/\omega^2)l_0^2 k_y$ is the center coordinate of the harmonic oscillator and $l_0 = \sqrt{\hbar/(m^*\omega_0)}$ is the harmonic oscillator length.

The numerical solution of the Schrödinger equation is performed by the finite element method (FEM), which is based on expressing the wave function as a linear combination of interpolation polynomials multiplied by as-yet-unknown coefficients in each of these elements.[35,36] We consider the harmonic oscillator length l_0 as a length scale and consecutively all energies are calculated in terms of $\hbar\omega_0$.

3. Results

3.1. Energy bands

To clarify the interplay of different SO interaction contributions, first of all, we calculate the energy dispersion relations of the subbands for various strengths of Rashba and Dresselhaus SO couplings without a magnetic field. Thereafter, we take into consideration the external magnetic field and calculate the energy bands to see how the magnetic field affects the subbands.

We can distinguish Rashba and Dresselhaus SO interactions into two regimes: weak $l_{so} \gg l_0$ and strong $l_{so} \lesssim l_0$ where $l_{so}^{R(D)} = \hbar^2/2m^*\alpha(\beta)$ is the length associated with SO couplings. In the presence of both types of SO couplings or only one type, the eigenenergies of the system are uniformly shifted downward by the total characteristic SO energy $\Delta_{so}^{T} = \Delta_{so}^{R} + \Delta_{so}^{D}$ where $\Delta_{so}^{R} = m^*\alpha^2/2\hbar^2$ and $\Delta_{so}^{D} = m^*\beta^2/2\hbar^2$ denote the Rashba and Dresselhaus SO couplings, respectively.[5,6]

3.1.1. Without magnetic field ($B = 0$)

With individual SO interaction ($\alpha \neq 0$ and $\beta = 0$) Initially, in order to identify the effect of individual SO coupling, in Fig. 2(a), we present the energy level spectrum of the quantum wire for strong Rashba SO interaction in the absence of an external magnetic field. Solid curves denote the energy dispersion with an individual mechanism of SO interaction whereas the dash-dotted curves indicate the case for the absence of SO interaction.

When we calculate the energy dispersion for Rashba and Dresselhaus SO interaction individually, we get similar energy subband dispersions for each same characteristic SO energy. Therefore, we show the case which includes only the Rashba SO coupling contribution in Fig. 2(a).

In the case that both the external magnetic field and SO interaction terms are zero, all subbands are spin degenerate (the dash-dotted curves in Fig. 2(a)). As seen in Fig. 2(a), by inclusion of the Rashba SO interaction, spin-splitting occurs in doubly-degenerated energy bands at $k_y \neq 0$ and spin degeneracy is preserved only for eigenstates with $k_y = 0$. This can be explained on the basis of the dependency of the SO interaction to the electron momentum.[14] For a weak Rashba SO contribution, the coupling between different subbands does not take place clearly (see Fig. 1(a) in Ref. [29]). As the Rashba SO interaction parameter is strengthened to a stronger value, coupling between spin-split levels causes an intraband mixing.

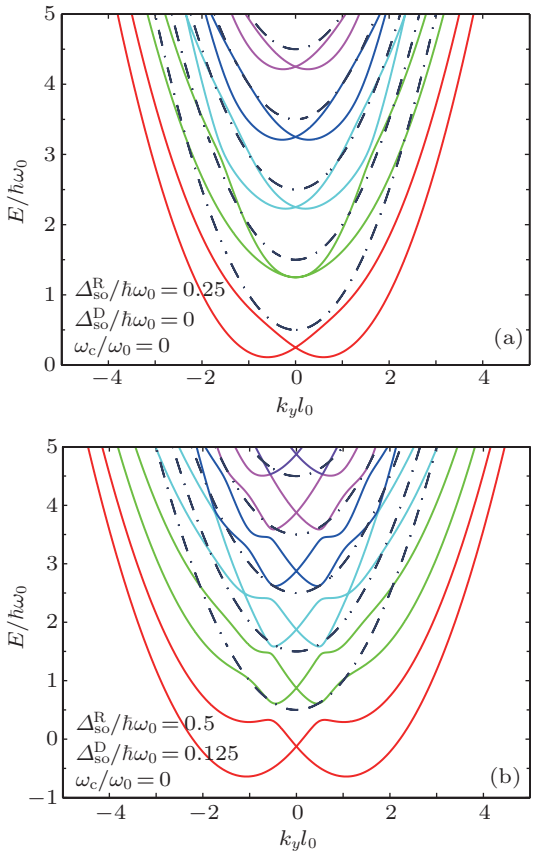


Fig. 2. (color online) Subband energy spectra of a quantum-wire for different Rashba and Dresselhaus SO strengths at zero magnetic field. (a) $\Delta_{so}^{R}/\hbar\omega_0 = 0.25$ and $\Delta_{so}^{D}/\hbar\omega_0 = 0$, (b) $\Delta_{so}^{R}/\hbar\omega_0 = 0.5$ and $\Delta_{so}^{D}/\hbar\omega_0 = 0.125$.

With the increase of the characteristic Rashba SO energy ($\Delta_{so}^{R}/\hbar\omega_0$), the parabolicity of the energy band is destroyed and coupling between neighbouring subbands rises. In the neighbourhood of $k_y = 0$, a "camel-back" shape arises from the effect of SO coupling for spin branches of lower energy levels, as seen in Fig. 2(b). For a stronger $\Delta_{so}^{R}/\hbar\omega_0$, described by the larger off-diagonal elements of the Hamiltonian matrix, significant coupling between neighbouring subbands leads to pronounced anticrossing (nonmonotonic portion) especially at higher levels. We should note that there is an energy shift in the subbands, which is proportional to the magnitude of SO coupling energy.

Interplay of both SO interaction ($\alpha \neq 0$ and $\beta \neq 0$) We calculate the energy levels of the quantum wire for Rashba and Dresselhaus SO couplings to determine how the simultaneous contribution of both of the SO interaction terms affect the energy dispersion.

The E–k_y curves for strong Rashba and Dresselhaus SO coupling regimes is given in Fig. 2(b). With inclusion of the

Dresselhaus term, the spin degeneracy is removed except the $k_y = 0$ point, as in the case for individual SO contribution (Fig. 2(a)); this term results in a downward energy shift at degeneracy point $k_y = 0$. In addition to this, for strong SO regimes, deviation from parabolicity of the subbands and anticrossing in higher subbands is visible. For weak Rashba and Dresselhaus SO interaction, the coupling between neighbouring subbands is not seen as clearly.

A comparison of Figs. 2(a) and 2(b) reveals that more pronounced anticrossings occur between subbands of different levels in the vicinity of $k_y = 0$ when both of the SO interaction terms coexist; we can say that the amount of downward shifting of energy increases with increasing the total characteristic SO coupling energy ($\Delta_{so}^{T}/\hbar\omega_0$).[5]

3.1.2. With magnetic field ($B \neq 0$)

To elucidate the interplay of the SO interaction with the magnetic field, at this point, we consider quantum wire subjected to a perpendicular magnetic field. As can be seen in the following figures, applying a magnetic field results in a subband separation and the degeneracy at $k_y = 0$ is removed.

In the absence of SO interaction ($\alpha = \beta = 0$) The dash-dotted curves in Fig. 3 show the energy level spectrum of electrons in a quantum wire without SO interactions for $k_y = 0$ as a function of ω_c/ω_0. When only the contribution of the magnetic field is considered, one can argue that the magnetic field lifts the degeneracy in each energy band by the Zeeman effect.

An increased magnetic field enhances the confinement potential, which results in it vertically upward shifting in the bottom of flattened energy subbands and increment in energy spacing between the upper and lower level of each subband (Refs. [5] and [29]).

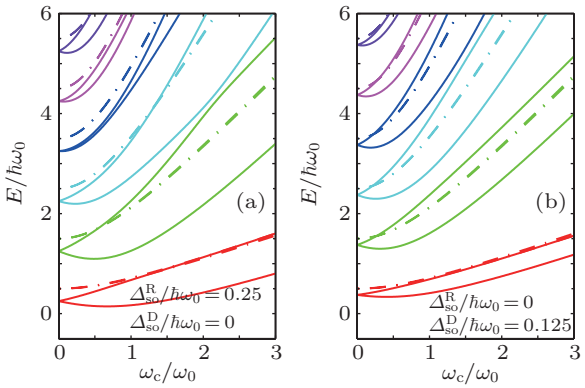


Fig. 3. (color online) Energy spectrum at $k_y = 0$ as a function of ω_c/ω_0 for individual mechanism of SO interaction. The dash-dotted lines indicate the energy dispersion in the absence of both SO coupling terms ($\Delta_{so}^{R}/\hbar\omega_0 = \Delta_{so}^{D}/\hbar\omega_0 = 0$). (a) Only the Rashba SO coupling term is taken into account: $\Delta_{so}^{R}/\hbar\omega_0 = 0.25$ and $\Delta_{so}^{D}/\hbar\omega_0 = 0$. (b) Only the Dresselhaus SO coupling term exists: $\Delta_{so}^{R}/\hbar\omega_0 = 0$ and $\Delta_{so}^{D}/\hbar\omega_0 = 0.125$.

In the presence of SO interaction ($\alpha \neq 0$ **and/or** $\beta \neq 0$) Next, we consider the case when both the SO interaction and the magnetic field are present. In order to illustrate to what extent the magnetic field modifies the energy dispersion, in Fig. 3(a), we present the energy subband dispersion of the quasi-1D quantum wire with a strong Rashba SO interaction as a function of ω_c/ω_0.

From Figs. 3(a) and 3(b), we obviously see varying separation between each energy subband branches due to the effect of the magnetic field as the index of the energy level increases. This separation also depends on the interplay between the SO coupling term and the externally applied magnetic field.

In order to illustrate the competing effect between Rashba and Dresselhaus SO interaction, we plot Fig. 4. Figures 4(a) and 4(d) represent the corresponding level spectrum with different and the same SO coupling strengths, respectively. For different coupling strengths, anticrossings between different subbands stand out, whereas for the same SO interaction strengths, crossings take place. In Figs. 4(b) and 4(e), the variation of the energy with respect to ω_c/ω_0 at $k_y = 0$ is given. In both figures, the different (same) amount of the contribution of SO interaction gives rise to a remarkable (unremarkable) separation of spin-up and spin-down branches of the energy states. When the magnetic field increases, the subband separation becomes larger owing to an increasing $\hbar\omega_c$ for small-indexes of energy levels. We also calculate the energy bands for different and the same Rashba and Dresselhaus SO coupling strengths in the presence of a strong magnetic field (Figs. 4(c) and 4(f)). The degeneracy at the point $k_y = 0$ that has been removed with the effect of the magnetic field is more evidently seen in a strong B-field regime. Higher magnetic field values cause the negligible anticrossing between the subbands and extinguish the "camel-back" shape of the lower energy subbands. For a fixed magnetic field, the magnitude of spin splitting between energy subbands of different states undergoes change. depending on the interplay of SO coupling and external magnetic field. Based on this observation and looking at the feature of Fig. 4(f), we can say that Rashba and Dresselhaus SO coupling terms can cancel each other by leading to a rather complex behavior in the energy dispersion in contrast with the different SO coupling strength cases.

With the assumption of a negligible intersubband crossing, the critical magnetic field for which the camelback shape ceases to exist can be described as $B_c = 2m^*\eta_{SOI}/(|g|\mu_B\hbar^2)$ where η_{SOI} represent α or β.[20,21] This fact reveals an important feature in energy dispersions: for cases with different SO interaction contributions, the camelback shape is preserved when the total effective magnetic field corresponding to SO interactions is greater than the applied magnetic field.

We obtain that the energy state spin-splitting strongly depends on the strengths of the Rashba and Dresselhaus SO coupling and also applied magnetic field.

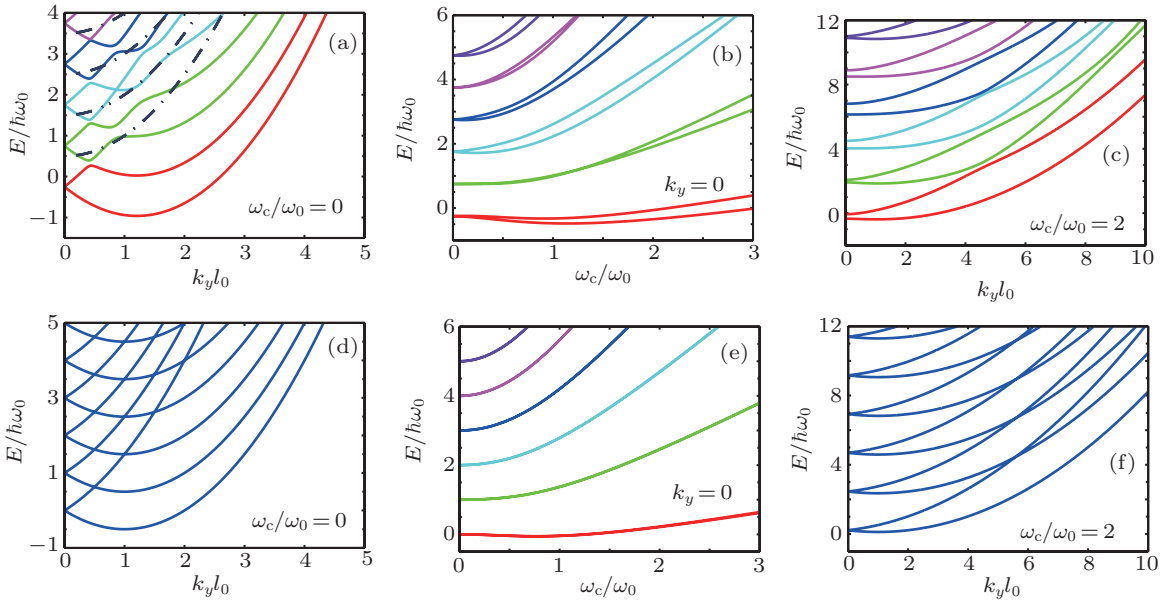


Fig. 4. (color online) (a) Energy subband dispersion at $B = 0$ with Rashba ($\Delta_{so}^{R}/\hbar\omega_0 = 0.5$) and Dresselhaus ($\Delta_{so}^{D}/\hbar\omega_0 = 0.25$) SO coupling effect. The dash-dotted curves indicate the case for the absence of SO interaction. (b) Energy spectrum of the same quantum wire at $k_y = 0$ as a function of ω_c/ω_0. (c) Energy dispersion of the wire at a finite magnetic field ($\omega_c/\omega_0 = 2$). (d)–(f) The same energy subband dispersion as in panels (a)–(c) with equal strength of Rashba and Dresselhaus SO interaction $\Delta_{so}^{R}/\hbar\omega_0 = \Delta_{so}^{D}/\hbar\omega_0 = 0.25$.

3.2. Wave functions

We plot the spinor components of the wave functions separately for the dimensionless wave vector values $k_y l_0$ for the first lowest spin-split subband in the presence and also absence of SO interactions.

Figure 5 shows the wave function of an electron in a finite magnetic field ($\omega_c/\omega_0 = 2$) without SO interaction. Skew direction of wave functions is determined by the Lorentz force associated with the magnetic field. Depending on whether the electrons are forward or backward traveling, this force deflects electrons toward either the left or the right edge of the quantum wire.[28]

By considering the x dependency of the real and imaginary parts of the spinor wave function, figure 5 emphasizes that $[\varphi_\uparrow(k_y,\ x)\ \ \varphi_\downarrow(k_y,\ x)]^{\mathrm{T}}$ can be separated in a spatial part and a space independent spinor part.

In Figs. 6–8, the real and imaginary parts of the spinor wave function are plotted separately $[\varphi_\uparrow(k_y,x)\ \ \varphi_\downarrow(k_y,x)]^{\mathrm{T}}$ for an electron in the lowest spin-split band under a strong magnetic field.

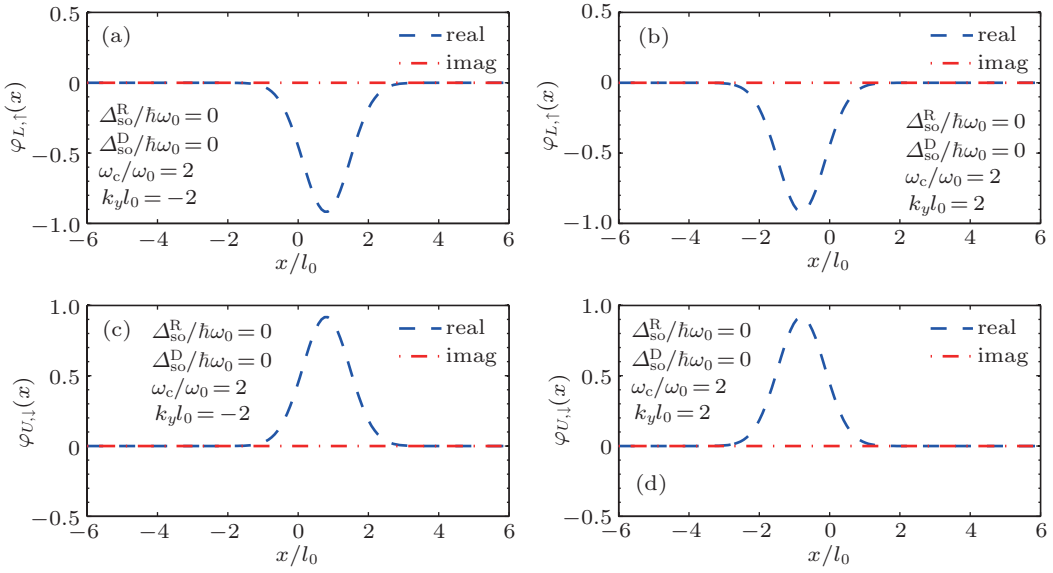


Fig. 5. (color online) Real and imaginary parts of the spinor wave function as a function of x/l_0 in the first subband for the case of a strong magnetic field ($\omega_c/\omega_0 = 2.0$) and the absence of SO interaction at $k_y l_0 = -2$ [panels (a) and (c)] and $k_y l_0 = 2$ [panels (b) and (d)]. The subscript L(U) indicates the lower(upper) spin-split level of the first subband.

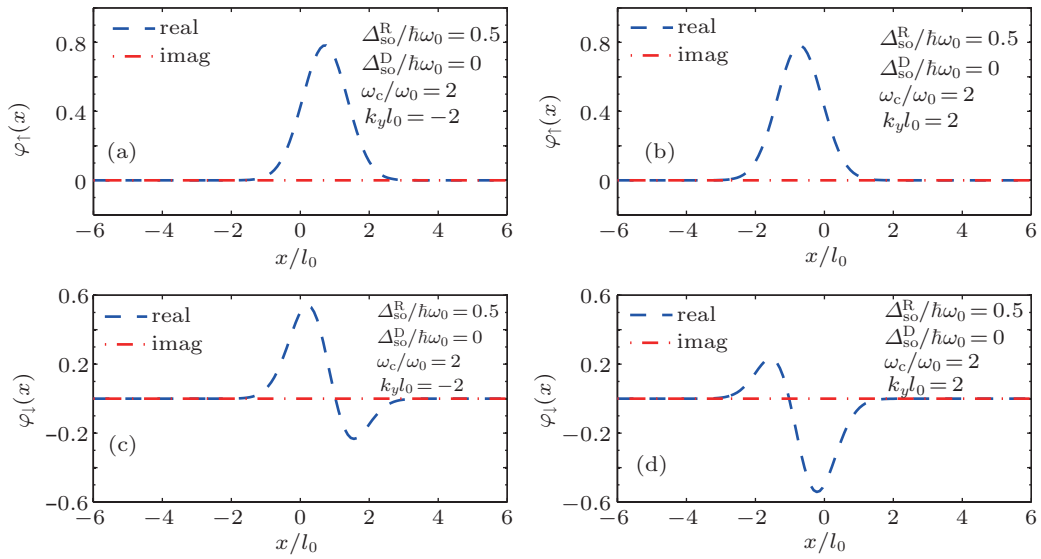


Fig. 6. (color online) Real and imaginary parts of the spinor wave function as a function of x/l_0 in the first subband when the quantum wire is under the effect of Rashba SO interaction ($\Delta_{so}^{R}/\hbar\omega_0 = 0.5$) and external magnetic field ($\omega_c/\omega_0 = 2$). (a) $\varphi_\uparrow(x)$ with $k_y l_0 = -2$, (b) $\varphi_\uparrow(x)$ with $k_y l_0 = 2$, (c) $\varphi_\downarrow(x)$ with $k_y l_0 = -2$, (d) $\varphi_\downarrow(x)$ with $k_y l_0 = 2$.

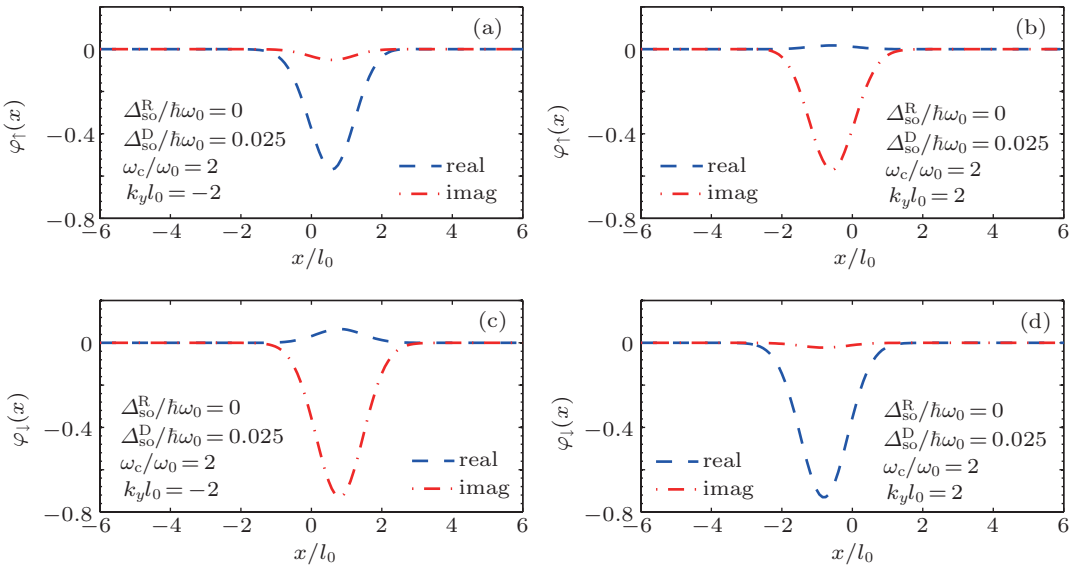


Fig. 7. (color online) Spinor wave function components as a function of x/l_0 for the lowest spin-split level in the presence of weak Dresselhaus SO interaction ($\Delta_{so}^{D}/\hbar\omega_0 = 0.025$) and strong magnetic field ($\omega_c/\omega_0 = 2$). (a) $\varphi_\uparrow(x)$ with $k_y l_0 = -2$, (b) $\varphi_\uparrow(x)$ with $k_y l_0 = 2$, (c) $\varphi_\downarrow(x)$ with $k_y l_0 = -2$, (d) $\varphi_\downarrow(x)$ with $k_y l_0 = 2$.

In the presence of Rashba and/or Dresselhaus SO coupling of any strength, a completely different emerging situation imposes the fact that the x dependent spinor wave function cannot be written as the product of the space dependent and eigenspinor part. This observation is in accordance with previous works in the literature.[21,24,25,28,37]

3.3. Spin orientation

The spin components of the eigenspinor $\varphi_n(k_y,x)$ in the n-th subband is given by

$$s_j^n(k_y,x) = [\varphi_{n,\uparrow}^*(k_y,x) \quad \varphi_{n,\downarrow}^*(k_y,x)]\,\sigma_j \cdot [\varphi_{n,\uparrow}(k_y,x) \quad \varphi_{n,\downarrow}(k_y,x)]^{\mathrm{T}}, \tag{9}$$

where $j = (x,y,z)$ and $[\varphi_{n,\uparrow}(k_y,x) \quad \varphi_{n,\downarrow}(k_y,x)]^{\mathrm{T}}$ is the spinor wave function in the n-th spin-split level; therefore, we can define "spin density" components $S_j^n(k_y,x)$ for a given k_y in the n-th level as[20,21]

$$S_j^n(k_y,x) = \frac{s_j^n(k_y,x)}{\sqrt{s_x^2(k_y,x)+s_y^2(k_y,x)+s_z^2(k_y,x)}}. \tag{10}$$

The spin density components depend on wave vector k_y, the level index $n(\uparrow,\downarrow)$ and also the confinement direction x. Consequently, for an electron belonging to a particular energy level with a certain wave vector k_y spin orientations will vary with location along the width of the quantum wire. This SO interaction-induced spatial modulation of the spin density across the wire width is known as "spin texturing".[20,37]

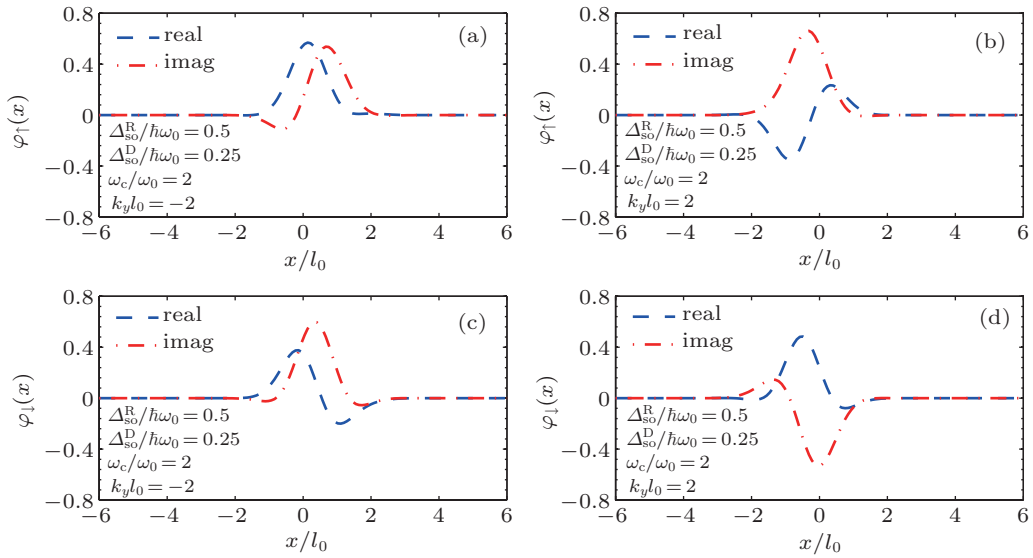


Fig. 8. (color online) The components of the spinor wave function when both SO interaction ($\Delta_{so}^{R}/\hbar\omega_0 = 2$ $\Delta_{so}^{D}/\hbar\omega_0 = 0.5$) and external magnetic field ($\omega_c/\omega_0 = 2$) are present. (a) $\varphi_\uparrow(x)$ with $k_y l_0 = -2$, (b) $\varphi_\uparrow(x)$ with $k_y l_0 = 2$, (c) $\varphi_\downarrow(x)$ with $k_y l_0 = -2$, (d) $\varphi_\downarrow(x)$ with $k_y l_0 = 2$.

In order to calculate the real-space spin density ($S_j(x)$), we need to merge the spin density contribution from all occupied states

$$S_j(x) = \sum_{n=1}^{N} \frac{\int_{k_{Fn}^-}^{k_{Fn}^+} S_j^n(k_y,x)\ \mathrm{d}k_y}{k_{Fn}^+ - k_{Fn}^-}, \quad j = (x,y,z), \qquad (11)$$

where N is the number of occupied spin-split levels whose bottoms are below the Fermi energy. In Eq. (11), intersection points between the Fermi energy and the $E - k_y$ curve on the right (left) denote k_{Fn}^+ (k_{Fn}^-) wave vectors of the n-th level. For the sake of simplicity, we assumed the low temperature limit, which means that only the states below the Fermi level are fully occupied.

The above definition (Eq. (11)) for real-space spin density can be used when the Fermi level intersects the subband only at two points, each of them locating at the opposite sides of the k_y axis. However, in a special case when the $E - k_y$ curve has a camelback shape, the Fermi level can intersect the same band at four different points. Thereby, Eq. (11) needs to be adjusted as follows:

$$S_j(x) = \frac{\int_{k_{F1}}^{k_{F2}} S_j(k_y,x)\ \mathrm{d}k_y}{k_{F2} - k_{F1}} + \frac{\int_{k'_{F1}}^{k'_{F2}} S_j(k_y,x)\ \mathrm{d}k_y}{k'_{F2} - k'_{F1}}. \qquad (12)$$

Here, k_{F1}, k_{F2} (k'_{F1}, k'_{F2}) are the wave vectors of intersection points between the Fermi level and the E–k_y curve on the left (right) of the energy axis.

In the following part, we present a detailed study of the spin texturing in a parabolically confined quantum wire with Rashba and/or Dresselhaus SO interaction and external magnetic field. We express our results in terms of $\rho_{1D} l_0$, which is the dimensionless form of the one-dimensional electron density (ρ_{1D}) across the wire and corresponding to densities in the range of 5×10^6–2×10^8 m^{-1}.[38]

3.3.1. Without SO interaction ($\alpha = \beta = 0$)

Initially, we investigated the case when only the existence of an external magnetic field causes vertical splitting of each subband. When only the lowest Zeeman-split band is occupied, one can foresee that $\hat{x}$ and $\hat{y}$ components ($S_x(x)$ and $S_y(x)$) of spin density will vanish even though $\hat{z}$ component ($S_z(x)$) will take a nonzero positive value due to the g-factor, in case of a strong magnetic field ($\omega_c/\omega_0 = 3.0$). The x-independence of the magnetic field leads to no spatial modulation of the spin density (Ref. [21]). We should state that if the system is under the effect of a moderate external magnetic field, such as ($\omega_c/\omega_0 = 0.3,\ 0.6$), all components of $\boldsymbol{S}(x)$ are zero since the g-factor is small.

When we consider the case where the Fermi level is above the bottom of the upper spin-split level of the first subband, the magnitude of the $S_z(x)$ will be almost zero according to Eq. (11). In other words, spins of the upper Zeeman branch are in the opposite direction with the lower Zeeman branch and therefore almost cancel each other out.

3.3.2. Without external magnetic field ($B = 0$)

Next, we want to illustrate to what extent the Rashba and Dresselhaus SO interaction effect modify the spin orientation. For this purpose, we calculate the spin textures for weak and strong SO interaction regimes. In this case, the spin-degenerate band is split into two horizantally displaced branches under the influence of SO coupling terms and the system has a degeneracy point at $k_y = 0$ (see Fig. 2).

In connection with the Rashba and Dresselhaus SO coupling effects, there exist effective Rashba ($\boldsymbol{B}_{\rm R}$) and Dresselhaus ($\boldsymbol{B}_{\rm D}$) pseudomagnetic fields, respectively, which give the contribution to the net magnetic field. The direction of the Rashba magnetic field is perpendicular to the $\hat{y}$ directed electron velocity and electric field associated with the Rashba effect that is in the $\hat{z}$ direction.[20,37,39,40] The effective Dresselhaus magnetic field is k_y dependent and oriented along the wire axis ($\hat{y}$).[21,41,42]

When only the lowest spin-split band is occupied (small electron density limit) and weak SO interaction regime is considered, we see that there is not any spatial modulation because of the weak coupling effects between the spin-split subbands. For weak Rashba (Dresselhaus) SO interaction, there is no magnetic field along $\hat{y}$ or $\hat{z}$ ($\hat{x}$ or $\hat{z}$), so $\boldsymbol{S}(x)$ components along these directions are zero. On the other hand, nonmagnetic feature of the material also results in zero $S_x(x)$ ($S_y(x)$). Similar behavior is obtained when both SO interaction terms are taken into account that can be explained by the afore mentioned reasons.

3.3.3. In the presence of both SO interaction ($\alpha \neq 0$, $\beta \neq 0$) and external magnetic field ($B \neq 0$)

In this case, the system is under the influence of $\hat{x}$ and $\hat{y}$ directed effective magnetic fields caused by Rashba and Dresselhaus SO interaction terms, in addition to the applied external magnetic field. As a consequence of that, components of $\boldsymbol{S}(x)$ have nonzero values along all three different $(\hat{x},\hat{y},\hat{z})$ directions. The spin orientation will vary based on the relative values of characteristic Rashba and Dresselhaus SO energies, and also external magnetic field. Pseudomagnetic fields due to SO interactions are k_y dependent.[20,21,41,42]

Low electron densities This density limit means that only the lowest spin-split subband of the first energy level lies below the Fermi energy. For different magnetic field values, we get real-space spin textures in the presence of weak Rashba and Dresselhaus SO coupling strengths, as shown in Fig. 9.

The $\hat{x}$ and $\hat{y}$ components of $\boldsymbol{S}(x)$ are zero at the center of the wire since they experience no $\boldsymbol{B}_{\rm R}$ and $\boldsymbol{B}_{\rm D}$, and they take different signs at opposite edges of the wire. The $\hat{z}$ component has minimum values near the two edges and reaches a maximum value at the center of the wire, in that the net magnetic field is $\hat{z}$ directed. The magnitude of all spin components increases with an increasing external magnetic field.

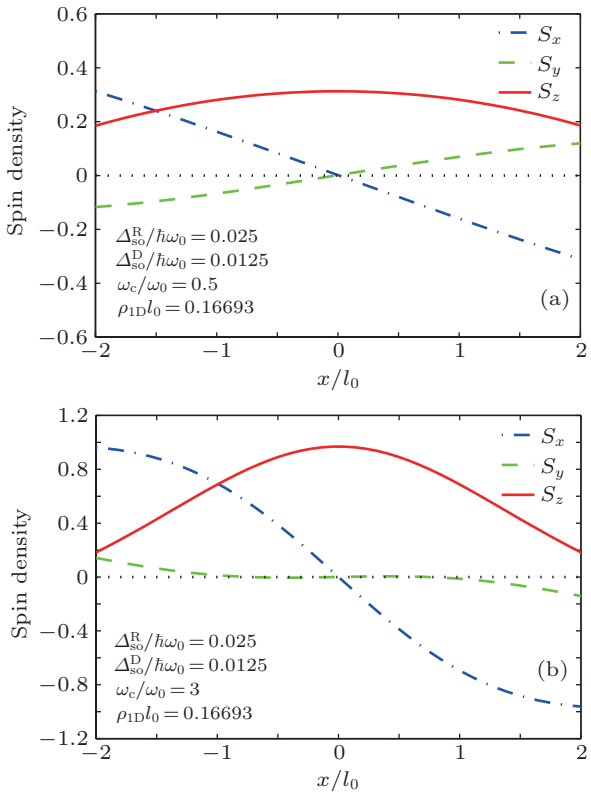


Fig. 9. (color online) Spatial variation of spin density components in the presence of weak Rashba and Dresselhaus SO coupling strengths ($\Delta_{\rm so}^{\rm R}/\hbar\omega_0 = 0.025$, $\Delta_{\rm so}^{\rm D}/\hbar\omega_0 = 0.0125$) at different magnetic fields, (a) $\omega_{\rm c}/\omega_0 = 0.5$, (b) $\omega_{\rm c}/\omega_0 = 3$. We consider the case when only the lowest spin-split band is occupied.

In the strong Rashba and Dresselhaus SO coupling regime, at first, we consider that the external magnetic field effect has a moderate strength ($\omega_{\rm c}/\omega_0 = 0.5$). As one can see in Fig. 10(a), $\hat{x}$ and $\hat{y}$ components of $\boldsymbol{S}(x)$ are zero at the center of the wire and both of them have opposite signs at the two edges. The $\hat{z}$ component of spin has minimum values near the edges and reaches a maximum value in the region close to the wire-center. On the other hand, with stronger SO interaction strengths, the spin distribution behaves more oscillatory that causes shortening in the "wavelength" of the standing wave of spin components, as can be seen from Figs. 9(b) and 10(b).

A qualitative explanation of the features in Fig. 10 could be as follows: pseudomagnetic Rashba field is proportional to translational velocity of electrons whereas Dresselhaus field is $\boldsymbol{k}_y$ dependent. Therefore, centrally localized electrons will experience neither a Rashba nor a Dresselhaus effective magnetic field. The only field exerted on the electrons at the center is the external one that leads to only one nonzero valued spin component ($S_z(x)$). In spite of that, different situations come out at the edges of the wire where anymore $\boldsymbol{B}_{\rm R}(x)$ and $\boldsymbol{B}_{\rm D}(x)$ are different than zero. Electrons located near the different edge points have oppositely directed translational velocities. Furthermore, $S_x(x)$ and $S_y(x)$ spin components will line up parallel to $\boldsymbol{B}_{\rm R}(x)$ and $\boldsymbol{B}_{\rm D}(x)$ to produce maximums with opposite signs at opposite edges of the wire.

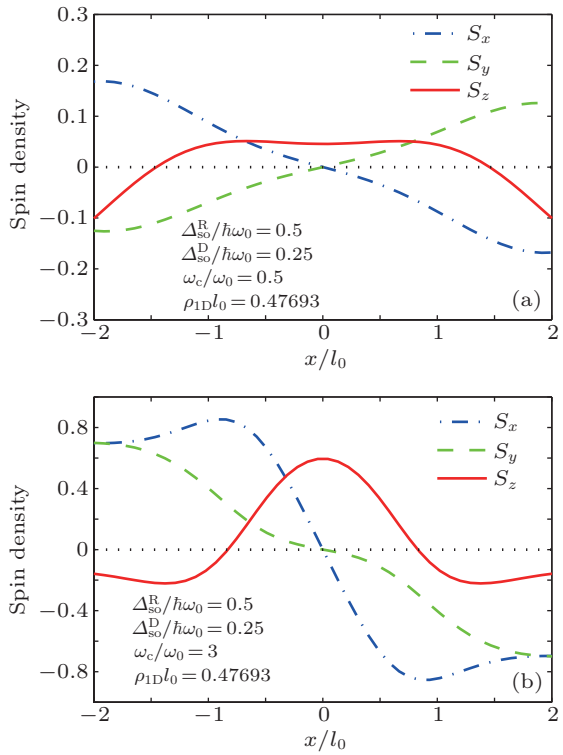


Fig. 10. (color online) Spin texture for the strong Rashba and Dresselhaus SO couplings ($\Delta_{so}^R/\hbar\omega_0 = 0.5$, $\Delta_{so}^D/\hbar\omega_0 = 0.25$). Magnetic field is varied from weak to strong limit, (a) $\omega_c/\omega_0 = 0.5$, (b) $\omega_c/\omega_0 = 3$, respectively. The lowest spin-split band at $\hbar\omega_0 = 2$ meV is occupied in all cases.

If we consider the system when it is under the effect of a strong magnetic field ($\omega_c/\omega_0 = 3.0$), we can get the spin textures as shown in Fig. 10(b); $S_x(x)$ has similar features with the moderate B case, whereas the $S_y(x)$ component undergoes a sign reversal. This behavior can be attributed to the flattening of the camelback shape in the energy spectrum with external field increasing.

Another important observation is that in the presence of both SO coupling terms, the S_z component of the spin orientation shows positional variation with respect to x, regardless of the SO coupling strengths. Meanwhile, stronger SO interaction limits cause more pronounced modulation, both in spatial behavior and sign reversal of all spin components.

High electron densities In this case, we analyze the treatment of the spin components when both of the lower and the upper spin-split branches of the lowest subband are occupied.

In Fig. 11, we show the spin distribution for a strong SO interaction for different magnetic fields ($\omega_c/\omega_0 = 0.5$ and $\omega_c/\omega_0 = 3$). At the center of the wire, electrons are oriented along the external magnetic field because of the fact that the net field comprises only of the applied magnetic field. Therefore, the $\hat{z}$ component of $\boldsymbol{S}(x)$ takes a higher value at the wire center. Besides $S_x(x)$ and $S_y(x)$ have zero value at the wire center and take opposite signs at different edge points since the values of $\boldsymbol{B}_R$ and $\boldsymbol{B}_D$ effective magnetic fields will increase for the electrons that are far away from the center of the wire. The magnitude of all spin components takes greater values when the applied magnetic field increases. The common feature in Fig. 11 reveals the fact that competing effects between different magnetic fields lead to more complicated oscillating behavior in spin distribution. Comparison between different density cases shows that for the high density limit, rapid spatial variation of all spin components is more evident than the low density case.

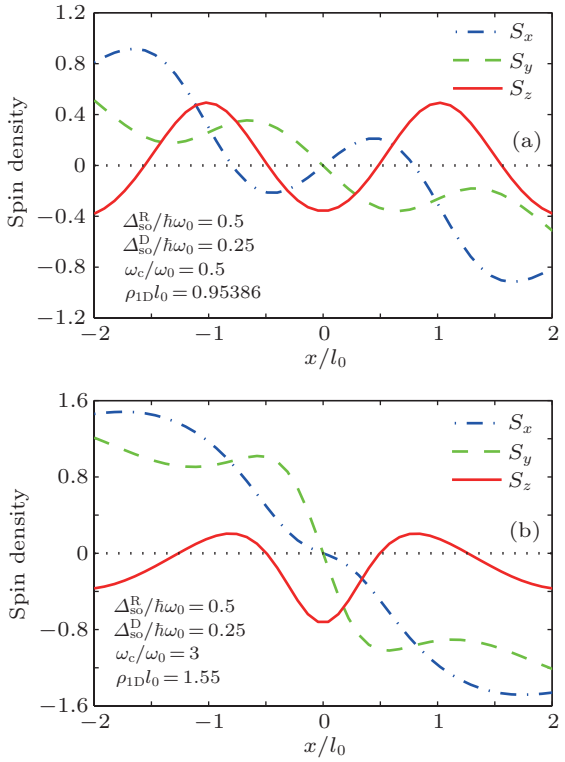


Fig. 11. (color online) Spin texture for the case when both spin-split branches of the lowest subband are occupied. Strong Rashba and Dresselhaus SO couplings case ($\Delta_{so}^R/\hbar\omega_0 = 0.5$, $\Delta_{so}^D/\hbar\omega_0 = 0.25$) is considered for two different values of magnetic field: (a) $\omega_c/\omega_0 = 0.5$, (b) $\omega_c/\omega_0 = 3$.

4. Conclusion

We have investigated the effect of a perpendicular magnetic field on the subband structure and spin texturing of a parabolically confined quantum wire, taking into account Rashba and Dresselhaus SO couplings. We find that the interplay between the magnetic field and SO couplings affects strongly the energy dispersion of the wire. Our numerical calculations show that the spatial distribution of the spin components can be modulated by the SO coupling, the external magnetic field and the carrier concentration of the system. We expect that these observations can assist in understanding the transport and optical properties of quasi-1D quantum structures.

Acknowledgment

One of the authors (S. Sarıkurt) would like to thank the Scientific and Technological Research Council of Turkey (TÜBİTAK) for their partial financial support. This work has been completed at the Dokuz Eylül University, Graduate School of Natural and Applied Sciences and is the subject of the forthcoming Ph.D. Thesis of S. Sarıkurt.

References

[1] Bader S D and Parkin S S P 2010 *Annu. Rev. Condens. Matter Phys.* **1** 71
[2] Fabian J, Matos-Abiaguea A, Ertlera C, Stano P and Žutić I 2007 *Acta Physica Slovaca* **57** 565
[3] Žutić I, Fabian J and Das Sarma S 2007 *Rev. Mod. Phys.* **76** 323
[4] Malet F, Pi M, Barranco M, Serra L and Lipparini E 2007 *Phys. Rev. B* **76** 115306
[5] Zhang S, Liang R, Zhang E, Zhang L and Liu Y 2006 *Phys. Rev. B* **73** 155316
[6] Knobbe J and Schäpers T 2005 *Phys. Rev. B* **71** 035311
[7] Rashba E I 1960 *Fiz. Tverd. Tela (Leningrad)* 2 1224
[8] Rashba E I 1960 *Sov. Phys. Solid State* **2** 1109
[9] Dresselhaus G 1955 *Phys. Rev.* **100** 580
[10] Winkler R 2003 *Spin Orbit Coupling Effects in Two-Dimensional Electron and Hole Systems* (Berlin: Springer-Verlag)
[11] Chang M C 2005 *Phys. Rev. B* **71** 085315
[12] Bulaev D V and Loss D 2005 *Phys. Rev. B* **71** 205324
[13] Krich J J and Halperin B I 2007 *Phys. Rev. Lett.* **98** 226802
[14] Debald S and Kramer B 2005 *Phys. Rev. B* **71** 115322
[15] Schäpers T, Guzenko V A, Bringer A, Akabori M, Hagedorn M and Hardtdegen H 2009 *Semicond. Sci. Technol.* **24** 064001
[16] Chang R S, Chu C S and Malśhukov A G 2009 *Phys. Rev. B* **79** 195314
[17] Schliemann J, Egues J C and Loss D 2003 *Phys. Rev. Lett.* **90** 146801
[18] Serra L, Sánchez D and López R 2005 *Phys. Rev. B* **72** 235309
[19] Giglberger S, Golub L E, Belḱov V V, Danilov S N, Schuh D, Gerl C, Rohlfing F, Stahl J, Wegscheider W, Weiss D, Prettl W and Ganichev S D 2007 *Phys. Rev. B* **75** 035327
[20] Upadhyaya P, Pramanik S, Bandyopadhyay S and Cahay M 2008 *Phys. Rev. B* **77** 045306
[21] Gujarathi S, Alam K M and Pramanik S 2012 *Phys. Rev. B* **85** 045413
[22] Governale M and Zülicke U 2002 *Phys. Rev. B* **66** 073311
[23] Governale M and Zülicke U 2004 *Solid State Commun.* **131** 581
[24] Moroz A V and Barnes C H W 1999 *Phys. Rev. B* **60** 14272
[25] Moroz A V and Barnes C H W 2000 *Phys. Rev. B* **61** R2464
[26] Mireles F and Kirczenow G 2001 *Phys. Rev. B* **64** 024426
[27] Perroni C A, Bercioux D, Ramaglia V M and Cataudella V 2007 *J. Phys.: Condens. Matter* **19** 186227
[28] Pramanik S, Bandyopadhyay S and Cahay M 2007 *Phys. Rev. B* **76** 155325
[29] Zhang T Y, Zhao W and Liu X M 2009 *J. Phys.: Condens. Matter* **21** 335501
[30] Erlingsson S I, Egues J C and Loss D 2010 *Phys. Rev. B* **82** 155456
[31] Gharaati A and Khordad R 2012 *Opt. Quantum Electron.* **44** 425
[32] Guzenko V A, Bringer A, Knobbe J, Hardtdegen H and Schäpers T 2007 *Appl. Phys. A* **87** 577
[33] Schäpers T, Knobbe J, Guzenko V A and van der Hart A 2004 *Physica E* **21** 933
[34] Schäpers T, Knobbe J and Guzenko V A 2004 *Phys. Rev. B* **69** 235323
[35] Pask J E, Klein B M, Sterne P A and Fong C Y 2001 *Comput. Phys. Commun.* **135** 1
[36] Ram-Mohan L R 2002 *Finite Element and Boundary Element Applications in Quantum Mechanics* (London: Oxford University Press)
[37] Upadhyaya P, Pramanik S and Bandyopadhyay S 2008 *Phys. Rev. B* **77** 155439
[38] Malet F, Pi M, Barranco M and Lipparini E 2005 *Phys. Rev. B* **72** 205326
[39] Cummings A W 2009 *The Spin Hall Effect in Quantum Wires* (Ph.D. Thesis) (Arizona State University)
[40] Camenzind L 2012 *Quantum Transport Signatures of Electric Dipole Spin Resonance Near the Persistent Spin Helix in GaAs Quantum Wells* (M.Sc. Thesis) (Basel: University of Basel)
[41] Meier L, Salis G, Gini E, Shorubalko I and Ensslin K 2008 *Phys. Rev. B* **77** 035305
[42] Studer M, Walser M P, Baer S, Rusterholz H, Schön S, Schuh D, Wegscheider W, Ensslin K and Salis G 2010 *Phys. Rev. B* **82** 235320